Superscaling analysis of inclusive electron scattering and its extension to charge-changing neutrino-nucleus cross sections beyond the relativistic Fermi gas approach

A. N. Antonov,[1] M. V. Ivanov,[1] M. K. Gaidarov,[1] E. Moya de Guerra,[2,3] J. A. Caballero,[4] M. B. Barbaro,[5] J. M. Udias,[3] and P. Sarriguren[6]

[1]*Institute for Nuclear Research and Nuclear Energy, Bulgarian Academy of Sciences, Sofia 1784, Bulgaria*
[2]*Instituto de Estructura de la Materia, CSIC, Serrano 123, E-28006 Madrid, Spain*
[3]*Departamento de Fisica Atomica, Molecular y Nuclear, Facultad de Ciencias Fisicas, Universidad Complutense de Madrid, Madrid E-28040, Spain*
[4]*Departamento de Fisica Atomica, Molecular y Nuclear, Universidad de Sevilla, Apdo. 1065, E-41080 Sevilla, Spain*
[5]*Dipartimento di Fisica Teorica, Università di Torino and INFN, Sezione di Torino, Via P. Giuria 1, I-10125 Torino, Italy*
[6]*Instituto de Estructura de la Materia, CSIC, Serrano 123, 28006 Madrid, Spain*

(Received 3 July 2006; published 10 November 2006)

Superscaling analyses of inclusive electron scattering from nuclei are extended from the quasielastic processes to the delta excitation region. The calculations of (e, e') cross sections for the target nucleus ^{12}C at various incident electron energies are performed using scaling functions $f(\psi')$ obtained in approaches going beyond the mean-field approximation, such as the coherent density fluctuation model (CDFM) and the one based on the light-front dynamics method. The results are compared with those obtained using the relativistic Fermi gas (RFG) model and the extended RFG model (ERFG). Our method utilizes in an equivalent way both basic nuclear quantities, density and momentum distributions, showing their role for the scaling and superscaling phenomena. The approach is extended to consider scaling function for medium and heavy nuclei with $Z \neq N$ for which the proton and neutron densities are not similar. The asymmetry of the CDFM quasielastic scaling function is introduced, simulating in a phenomenological way the effects that violate the symmetry for $\psi' \geqslant 0$, including the role of the final-state interaction. The superscaling properties of the electron scattering are used to predict charge-changing neutrino-nucleus cross sections at energies from 1 to 2 GeV. A comparison with the results of the ERFG model is made. The analyses make it possible to gain information about the nucleon correlation effects on both local density and nucleon momentum distributions.

DOI: 10.1103/PhysRevC.74.054603 PACS number(s): 25.30.−c, 21.60.−n, 25.30.Pt, 21.10.Ft

I. INTRODUCTION

Over the past four decades electron scattering has provided a wealth of information on nuclear structure and dynamics. Form factors and charge distributions have been extracted from elastic scattering data, whereas inelastic measurements have allowed for a systematic study of the dynamic response over a broad range of momentum and energy transfer. The nuclear y-scaling analysis of inclusive electron scattering from a large variety of nuclei (e.g., Refs. [1–10]) showed the existence of high-momentum components in the nucleon momentum distributions $n(k)$ at momenta $k > 2$ fm^{-1} due to the presence of nucleon-nucleon (NN) correlations. It was shown (see, e.g., Refs. [11–15]) that this specific feature of $n(k)$, which is similar for all nuclei, is a physical reason for the scaling and superscaling phenomena in nuclei.

The concepts of scaling [1–9] and superscaling [10–16] have been explored in Refs. [12,17] for extensive analyses of the (e, e') world data (see also Ref. [18]). Scaling of the first kind (no dependence on the momentum transfer) is reasonably good as expected, at excitation energies below the quasielastic (QE) peak, whereas scaling of second kind (no dependence on the mass number) is excellent in the same region. When both types of scaling behavior occur one says that superscaling takes place. At energies above the QE peak both scaling of the first and, to a lesser extent, of the second kind are shown to be violated because of important contributions introduced by effects beyond the impulse approximation, namely inelastic scattering [19,20] together with correlation contributions and meson exchange currents [21,22].

The superscaling analyses of inclusive electron scattering from nuclei for relatively high energies (several hundred MeV to a few GeV) have recently been extended to include not only quasielastic processes but also the region where Δ excitation dominates [23]. A good representation of the electromagnetic response in both quasielastic and Δ regions has been obtained using the scaling ideas, importantly, with an asymmetric QE scaling function $f^{\mathrm{QE}}(\psi')$ (ψ' is the scaling variable in the QE region) and a scaling function $f^{\Delta}(\psi'_{\Delta})$ in the region up to inelasticities where the Δ contribution reaches its maximum. Both functions were deduced from phenomenological fits to electron-scattering data. Particularly, for the scaling function in the quasielastic region it has been shown in Ref. [23] that, in contrast to the relativistic Fermi gas model scaling function, which is symmetric, limited strictly to the region $-1 \leqslant \psi' \leqslant +1$, and with a maximum value 3/4, the empirically determined $f^{\mathrm{QE}}(\psi')$ has a somewhat asymmetric shape with a tail that extends toward positive values of ψ' and its maximum is only about 0.6. Of course, the specific features of the scaling function should be accounted for by reliable microscopic calculations that take final-state iterations (FSI) into account. In particular, the asymmetric shape of f^{QE} tested in Refs. [24,25] by using a relativistic

mean field (RMF) for the final states shows a very good agreement with the behavior presented by the experimental scaling function.

The superscaling analyses and the present knowledge of inclusive electron scattering allowed one to start studies of neutrino scattering off nuclei on the same basis. The reactions of incident neutrino beams interacting with a complex nucleus have offered unique opportunities for exploring fundamental questions in different domains in physics. Recently, positive signals of neutrino oscillations confirmed the hypothesis of nonzero neutrino masses and triggered much interest on this issue [26]. To better analyze the next generation of high-precision neutrino oscillation experiments and to reduce their systematic uncertainty both neutral- (e.g., Refs. [27–31]) and charged-current (e.g., Refs. [23,24,29,30,32–37]) neutrino-nucleus scattering have stimulated detailed investigations.

The neutrino-nucleus interactions have been studied within several approaches investigating a variety of effects. Using the superscaling analysis of few-GeV inclusive electron-scattering data, a method was proposed in Ref. [23] to predict the inclusive νA and $\bar{\nu}A$ cross sections for the case of ^{12}C in the nuclear resonance region, thereby effectively including Δ isobar degrees of freedom. It was shown in Refs. [27,34] that the important final-state interaction effects arising from the use of relativistic optical potentials within a relativistic Green's function approach lower the cross section by at least a 14% factor at incoming neutrino energies of 1 GeV. A similar result has been obtained in Refs. [38,39], where the use of random-phase approximation (RPA) to predict the neutrino-nucleus cross section was discussed. Apart from relativistic dynamics and FSI, other effects may influence the neutrino-nucleus reactions. The role of Pauli blocking and FSI in charged-current neutrino induced reactions is analyzed in Refs. [35–37].

In this article we follow our method presented in Refs. [13–15] to calculate the scaling function in finite nuclei first within the coherent density fluctuation model (e.g., Refs. [40–43]). This approach, which is a natural extension of the relativistic Fermi gas (RFG) model, has shown how both basic quantities, density and momentum distributions, are responsible for the scaling and superscaling phenomena in various nuclei. Although the scaling function obtained in Ref. [13] is symmetrical around $\psi' = 0$, the results agree with the available experimental data at different transferred momenta and energies below the quasielastic peak position, showing superscaling for $\psi' < 0$, including $\psi' < -1$, whereas in the RFG model $f(\psi') = 0$ for $\psi' \leqslant -1$. It was shown in Ref. [14] that the QE scaling function can be obtained within the coherent density fluctuation model (CDFM) in two equivalent ways, on the basis of the local density distribution, as well as of the nucleon momentum distribution. As pointed out in Ref. [14], the nucleon momentum distributions $n(k)$ for various nuclei obtained in Ref. [44] within a parameter-free theoretical approach based on the light-front dynamics method (e.g., Refs. [45,46] and references therein) can also be used to describe both y and ψ'-scaling data. So, in our present work we explore both methods, CDFM and light-front dynamics (LFD), to investigate further the scaling functions and their applications to analyses of electron and neutrino scattering off nuclei.

Our work is motivated by the fact that different models of the nuclear dynamics (including those with RMF dynamics and with RPA-type correlations accounted for) describe with different success the basic size and shape of the cross sections in studies of high-energy inclusive lepton scattering used so far. For this reason we extend further our consideration and calculate within the CDFM and LFD the scaling functions in the kinematical regions of the QE and Δ peak on the basis of momentum and density distributions of finite nuclear systems in which nucleon correlations are included. This can be done either by using available empirical data for these quantities or theoretical calculations in which correlations are included to some extent. Then, the obtained scaling functions are applied to calculate electron-nucleus cross sections in QE and Δ regions in the energy range from 500 MeV to 2 GeV for the target nucleus ^{12}C and to predict charge-changing neutrino and antineutrino reaction cross sections from the scaling region to the QE peak at energies of few GeV. We also make comparisons of the results obtained using our methods with those obtained using the RFG model and other theoretical schemes.

The article is organized in the following way. In Sec. II we present the formalism needed in studies of scaling functions in the quasielastic region and validate the superscaling within the CDFM and LFD for a variety of nuclei with $Z = N$ and $Z \neq N$. Then, we consider the nucleon momentum distributions and their applications in both approaches showing the sensitivity of the calculated scaling functions to the peculiarities of $n(k)$ in different regions of momenta. Section III contains the CDFM and LFD methods to build up the scaling function in the Δ region. The formalism involved in obtaining the electron-nucleus cross sections in QE and Δ kinematical regions and the results of the numerical calculations are presented in Sec. IV A. In Sec. IV B we give our theoretical predictions for cross sections of quasielastic charge-changing neutrino reactions. Finally, in Sec. V we summarize the results of our work.

II. SCALING FUNCTION IN THE QUASIELASTIC REGION

A. QE scaling function in the CDFM

As already mentioned in the Introduction, the superscaling behavior was first considered within the framework of the RFG model [10–12,16,17,19], where a properly defined function of the ψ' variable was introduced. As pointed out in Ref. [12], however, the actual nuclear dynamical content of the superscaling is more complex than that provided by the RFG model. It was observed that the experimental data have a superscaling behavior in the low-ω side (ω being the transfer energy) of the quasielastic peak for large negative values of ψ' (up to $\psi' \approx -2$), whereas the predictions of the RFG model are $f(\psi') = 0$ for $\psi' \leqslant -1$. This imposes the consideration of the superscaling in realistic finite systems. One of the approaches to do this was developed [13,14] in the CDFM [40–43] that is related to the δ-function limit of the generator coordinate method [13,47]. It was shown in Refs. [13–15] that the superscaling in nuclei can be explained quantitatively on the basis of the similar behavior of the high-momentum components of the nucleon momentum distribution in light,

medium, and heavy nuclei. As already mentioned, the latter is related to the effects of the *NN* correlations in nuclei (see, e.g., Refs. [40,41]).

The scaling function in the CDFM was obtained starting from that in the RFG model [10–12,16] in two equivalent ways: on the basis of the local density distribution $\rho(r)$ and of the nucleon momentum distribution $n(k)$. This allows one to study simultaneously the role of the *NN* correlations included in $\rho(r)$ and $n(k)$ in the case of the superscaling phenomenon. To explore these properties the scaling function $f(\psi')$ has been derived in two ways in CDFM in Ref. [14]. First, by means of the density distribution $\rho(r)$, it leads to

$$f^{\mathrm{QE}}(\psi') = \int_0^{\alpha/(k_F|\psi'|)} dR|F(R)|^2 f^{\mathrm{QE}}_{\mathrm{RFG}}[\psi'(R)], \tag{1}$$

with a weight function of the form

$$|F(R)|^2 = -\frac{1}{\rho_0(R)} \left.\frac{d\rho(r)}{dr}\right|_{r=R}, \tag{2}$$

where

$$\rho_0(R) = \frac{3A}{4\pi R^3}. \tag{3}$$

$f^{\mathrm{QE}}_{\mathrm{RFG}}[\psi'(R)]$ with $\psi'(R) = k_F R\psi'/\alpha$ is the scaling function related to the RFG model

$$f^{\mathrm{QE}}_{\mathrm{RFG}}[\psi'(R)] = \frac{3}{4}\left[1-\left(\frac{k_F R|\psi'|}{\alpha}\right)^2\right]\left\{1+\left(\frac{Rm_N}{\alpha}\right)^2\left(\frac{k_F R|\psi'|}{\alpha}\right)^2 \times\left[2+\left(\frac{\alpha}{Rm_N}\right)^2-2\sqrt{1+\left(\frac{\alpha}{Rm_N}\right)^2}\right]\right\}, \tag{4}$$

m_N being the nucleon mass and $\alpha = (9\pi A/8)^{1/3} \simeq 1.52A^{1/3}$. Second, by means of the momentum distribution $n(k)$, the scaling function is expressed by

$$f^{\mathrm{QE}}(\psi') = \int_{k_F|\psi'|}^{\infty} d\bar{k}_F |G(\bar{k}_F)|^2 f^{\mathrm{QE}}_{\mathrm{RFG}}[\psi'(\bar{k}_F)], \tag{5}$$

where $\psi'(\bar{k}_F) = k_F\psi'/\bar{k}_F$ and the weight function is

$$|G(\bar{k}_F)|^2 = -\frac{1}{n_0(\bar{k}_F)} \left.\frac{dn(k)}{dk}\right|_{k=\bar{k}_F} \tag{6}$$

with

$$n_0(\bar{k}_F) = \frac{3A}{4\pi \bar{k}_F{}^3}. \tag{7}$$

In Eq. (5) the RFG scaling function $f^{\mathrm{QE}}_{\mathrm{RFG}}[\psi'(\bar{k}_F)]$ can be obtained from $f^{\mathrm{QE}}_{\mathrm{RFG}}[\psi'(R)]$ [Eq. (4)] by changing α/R by $\bar{k}_F$. In Eqs. (1), (4), and (5) the Fermi momentum k_F is not a free parameter for different nuclei as it is in the RFG model, but k_F is calculated within the CDFM for each nucleus using the corresponding expressions:

$$k_F = \int_0^\infty dR k_F(R)|F(R)|^2 = \alpha\int_0^\infty dR\frac{1}{R}|F(R)|^2 = \frac{4\pi(9\pi)^{1/3}}{3A^{2/3}}\int_0^\infty dR\rho(R)R \tag{8}$$

when the condition

$$\lim_{R\to\infty}[\rho(R)R^2] = 0 \tag{9}$$

is fulfilled and

$$k_F = \frac{16\pi}{3A}\int_0^\infty d\bar{k}_F n(\bar{k}_F)\bar{k}_F{}^3 \tag{10}$$

when the condition

$$\lim_{\bar{k}_F\to\infty}\left[n(\bar{k}_F)\bar{k}_F{}^4\right] = 0 \tag{11}$$

is fulfilled.

As shown in Ref. [14], the integration in Eqs. (1) and (5), using Eqs. (2) and (6), leads to the explicit relationships of the scaling functions with the density and momentum distributions:

$$f^{\mathrm{QE}}(\psi') = \frac{4\pi}{A}\int_0^{\alpha/(k_F|\psi'|)} dR\rho(R) \times\left\{R^2 f^{\mathrm{QE}}_{\mathrm{RFG}}[\psi'(R)] + \frac{R^3}{3}\frac{\partial f^{\mathrm{QE}}_{\mathrm{RFG}}[\psi'(R)]}{\partial R}\right\} \tag{12}$$

and

$$f^{QE}(\psi') = \frac{4\pi}{A}\int_{k_F|\psi'|}^\infty d\bar{k}_F n(\bar{k}_F) \times\left\{\bar{k}_F{}^2 f^{\mathrm{QE}}_{\mathrm{RFG}}[\psi'(\bar{k}_F)] + \frac{\bar{k}_F{}^3}{3}\frac{\partial f^{\mathrm{QE}}_{\mathrm{RFG}}[\psi'(\bar{k}_F)]}{\partial \bar{k}_F}\right\}, \tag{13}$$

the latter at

$$\lim_{\bar{k}_F\to\infty}\left[n(\bar{k}_F)\bar{k}_F{}^3\right] = 0. \tag{14}$$

One can see the symmetry in both Eqs. (12) and (13) written in r- and k-space. We also note that in the consideration up to here the CDFM scaling function $f^{\mathrm{QE}}(\psi')$ is symmetric under the change of ψ' by -ψ'.

In Refs. [13,14] we used the charge density distributions to determine the weight function $|F(R)|^2$ and $f^{\mathrm{QE}}(\psi')$ in Eqs. (1), (2), and (8) for the cases of ^{4}He, ^{12}C, ^{27}Al, ^{56}Fe, and ^{197}Au. The results for the scaling function $f^{\mathrm{QE}}(\psi')$ agree well with the available data from the inclusive quasielastic electron scattering for ^{4}He, ^{12}C, ^{27}Al, and ^{56}Fe and only approximately for ^{197}Au for various values of the transfer momentum $q = 500, 1000, 1650$ MeV/c [13] and $q = 1560$ MeV/c [14], showing superscaling for negative values of ψ', including also those smaller than -1, whereas in the RFG model $f(\psi') = 0$ for $\psi' \leqslant -1$. One can see this in Fig. 1 for ^{4}He, ^{12}C, and ^{27}Al at $q = 1000$ MeV/c. At the same time, however, in Refs. [13,14] we encountered some difficulties to describe the superscaling in ^{197}Au, which was the heaviest nucleus considered. We related this in Refs. [13,14] to the particular A dependence of $n(k)$ in the model that does not lead to realistic high-momentum components of $n(k)$ in the

heaviest nuclei. We followed in Refs. [13,14] an artificial way to "improve" the high-momentum tail of $n(k)$ in ^{197}Au by taking the value of the diffuseness parameter b in the Fermi-type charge density distribution of this nucleus to be $b = 1$ fm instead of the value $b = 0.449$ fm (as obtained from electron elastic-scattering experiments, see, e.g., Ref. [48]). In this way the high-momentum tail of $n(k)$ for ^{197}Au in CDFM becomes similar to those of ^{4}He, ^{12}C, ^{27}Al, and ^{56}Fe and this leads to a good agreement of the scaling function $f^{\rm QE}(\psi')$ with the data also for ^{197}Au. In Ref. [13] we pointed out, however, that all the nucleons (not just the protons) may contribute to $f^{\rm QE}(\psi')$ for the transverse electron scattering and this could be simulated by increasing of the diffuseness of the matter density with respect to that of the charge density for a nucleus like ^{197}Au that has much larger number of neutron than of protons.

In Ref. [15] we assumed that the reason why the CDFM does not work properly in the case of ^{197}Au is that we had used in Refs. [13,14] only the phenomenological charge density, while this nucleus has many more neutrons than protons ($N = 118$ and $Z = 79$) and therefore, proton and neutron densities may differ considerably. In the case when $Z \neq N$ and the proton and neutron densities are not similar, the total scaling function will be expressed by the sum of the proton $f_p^{\rm QE}(\psi')$ and neutron $f_n^{\rm QE}(\psi')$-scaling functions, which are determined by the proton and neutron densities $\rho_p(r)$ and $\rho_n(r)$, respectively:

$$f^{\rm QE}_{p(n)}(\psi') = \int_0^{\alpha_{p(n)}/(k_F^{p(n)}|\psi'|)} dR|F_{p(n)}(R)|^2 f^{p(n)}_{\rm RFG}[\psi'(R)]. \quad (15)$$

In Eq. (15) the proton and neutron weight functions are obtained from the corresponding proton and neutron densities

$$\left|F_{p(n)}(R)\right|^2 = -\frac{4\pi R^3}{3Z(N)} \left.\frac{d\rho_{p(n)}(r)}{dr}\right|_{r=R}, \quad (16)$$

$$\alpha_{p(n)} = \left[\frac{9\pi Z(N)}{4}\right]^{1/3}, \quad (17)$$

$$\int_0^\infty \rho_{p(n)}(\vec{r})d\vec{r} = Z(N), \quad (18)$$

and the Fermi momentum for the protons and neutrons is given by

$$k_F^{p(n)} = \alpha_{p(n)} \int_0^\infty dR \frac{1}{R}|F_{p(n)}(R)|^2. \quad (19)$$

The RFG proton and neutron scaling functions $f^{p(n)}_{\rm RFG}[\psi'(R)]$ have the form of Eq. (4), where α and k_F stand for $\alpha_{p(n)}$ from Eq. (17) and $k_F^{p(n)}$ from Eq. (19), respectively. The functions are normalized as follows:

$$\int_0^\infty |F_{p(n)}(R)|^2 dR = 1, \quad (20)$$

$$\int_{-\infty}^\infty f^{QE}_{p(n)}(\psi')d\psi' = 1. \quad (21)$$

Then the total scaling function can be expressed by means of both proton and neutron scaling functions:

$$f^{\rm QE}(\psi') = \frac{1}{A}\left[Zf_p^{\rm QE}(\psi') + Nf_n^{\rm QE}(\psi')\right] \quad (22)$$

and is normalized to unity.

The same consideration can be performed equivalently on the basis of the nucleon momentum distributions for protons $n^p(k)$ and neutrons $n^n(k)$ presenting $f^{\rm QE}(\psi')$ by the sum of proton and neutron scaling functions (22) calculated similarly to Eqs. (15)–(22) [and to Eqs. (5), (6), (10), and (11)]:

$$f^{\rm QE}_{p(n)}(\psi') = \int_{k_F^{p(n)}|\psi'|}^\infty d\bar{k}_F |G_{p(n)}(\bar{k}_F)|^2 f^{p(n)}_{\rm RFG}[\psi'(\bar{k}_F)], \quad (23)$$

where

$$|G_{p(n)}(\bar{k}_F)|^2 = -\frac{4\pi \bar{k}_F{}^3}{3Z(N)} \left.\frac{dn^{p(n)}(k)}{dk}\right|_{k=\bar{k}_F} \quad (24)$$

with $f^{p(n)}_{\rm RFG}[\psi'(\bar{k}_F)]$ containing $\alpha_{p(n)}$ from Eq. (17) and $k_F^{p(n)}$ calculated as

$$k_F^{p(n)} = \int_0^\infty d\bar{k}_F \bar{k}_F |G_{p(n)}(\bar{k}_F)|^2. \quad (25)$$

The scaling functions for several examples, such as the medium stable nuclei ^{62}Ni and ^{82}Kr and the heavy nuclei ^{118}Sn and ^{197}Au are calculated following Eqs. (15)–(22) using the corresponding proton and neutron densities obtained in deformed self-consistent mean-field Hartree-Fock (HF) + BCS calculations with density-dependent Skyrme effective interaction (SG2) and a large harmonic-oscillator basis with 11 major shells [49,50]. In Fig. 1 we give the results for the ^{82}Kr and ^{197}Au nuclei in which $Z \neq N$ and compare them with the results for ^{4}He, ^{12}C ($Z = N$) and ^{27}Al ($Z \simeq N$), as well as with the experimental data (presented by a gray area and taken from Ref. [12]) obtained for ^{4}He, ^{12}C, ^{27}Al, ^{56}Fe, and ^{197}Au. The scaling functions are in a reasonable agreement with the data, which was not the case for ^{197}Au calculated in Ref. [13] by using only the Fermi-type charge density with phenomenological parameter values $b = 0.449$ fm and $R = 6.419$ fm from Ref. [48]. At the same time we note also the improvement in comparison with the RFG model result in which $f^{\rm QE}(\psi') = 0$ for $\psi' \leqslant -1$. Thus, it can be concluded that the scaling function $f^{\rm QE}(\psi')$ for nuclei

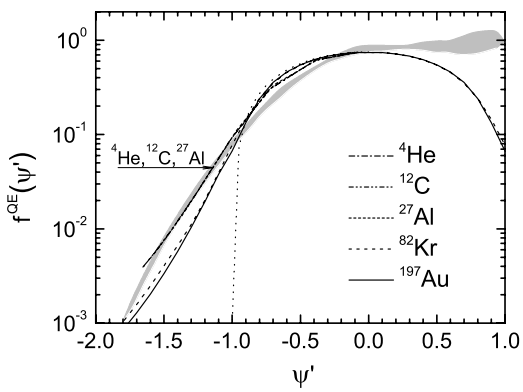

FIG. 1. The quasielastic scaling function $f^{\rm QE}(\psi')$ at $q = 1000$ MeV/c for ^{4}He, ^{12}C, ^{27}Al, ^{82}Kr, and ^{197}Au calculated in CDFM. (Dotted line) RFG model result. The curves for ^{4}He, ^{12}C, and ^{27}Al nuclei almost coincide. (Gray area) Experimental data [11,12].

with $Z \neq N$ for which the proton and neutron densities are not similar has to be expressed by the sum of the proton and neutron scaling functions. The latter can be calculated by means of theoretically and/or experimentally obtained proton and neutron local density distributions or momentum distributions.

As known (e.g., Refs. [12,23]), the total inclusive electron scattering response is assumed to be composed of several contributions: (i) the entire longitudinal contribution that superscales and is represented by the QE scaling function $f^{\rm QE}(\psi')$; (ii) a part of the transverse response, which arises from the quasielastic knockout of nucleons and is also driven by the scaling function $f^{\rm QE}(\psi')$; and (iii) the additional contribution of the transverse response from MEC effects and from inelastic single-nucleon processes, including the excitation of the Δ isobar. The effects of point (iii) break the scaling. In Ref. [23] a universal scaling function $f^{\rm QE}(\psi')$ has been determined by reliable separations of the empirical data into their longitudinal and transverse contributions for $A > 4$. Such separations are available only for a few nuclei [51]. All of these response functions have been used to extract the "universal" QE response function $f^{\rm QE}(\psi')$ (see Fig. 1 of Ref. [23]), which is parametrized by a simple function. This function has a somewhat asymmetric shape. Its left tail ($\psi' < 0$) passes through the gray area of Fig. 1. The right tail ($\psi' > 0$) extends larger toward positive values of ψ'. In contrast, the RFG scaling function is symmetric. The CDFM scaling function discussed so far, which is based on the RFG one, is also symmetric. As mentioned, the maximum value of $f^{\rm QE}(\psi')$ in RFG (and in CDFM) is 3/4, whereas the empirical scaling function extracted in Ref. [23] reaches about 0.6.

As mentioned in Ref. [23], if FSI are neglected, the RMF theory [33,52,53] and relativized shell-model studies [54] provide rather modest differences from the RFG predictions. Another possible reason for the differences between the RFG (or mean-field results) and the empirically determined scaling function arises from high-momentum components in realistic wave functions that may be large enough. In Ref. [23] the scaling function was taken from the experiment. In the present work we also limit our approach to phenomenology when considering the asymmetric shape and the maximum value of the quasielastic scaling function. To simulate the role of all the effects that lead to asymmetry, we impose the latter on the RFG scaling function (and, correspondingly, on the CDFM one) by introducing a parameter that gives the correct maximum value of the scaling function (c_1 in our expressions given below) and also an asymmetry in $f^{\rm QE}(\psi')$ for $\psi' \geqslant 0$. We consider the main parts of the RFG scaling function for $\psi' \leqslant 0$ and $\psi' \geqslant 0$ in the following forms, keeping the parabolic dependence on ψ' as required in Ref. [10]:

$$f^{\rm QE}_{{\rm RFG},1}(\psi') = c_1(1-\psi'^2)\Theta(1-\psi'^2), \qquad \psi' \leqslant 0, \tag{26}$$

$$f^{\rm QE}_{{\rm RFG},2}(\psi') = c_1\left[1-\left(\frac{\psi'}{c_2}\right)^2\right]\Theta\left[1-\left(\frac{\psi'}{c_2}\right)^2\right], \qquad \psi' \geqslant 0. \tag{27}$$

The total RFG scaling function is normalized to unity:

$$\int_{-\infty}^{\infty} f^{\rm QE}_{\rm RFG}(\psi')d\psi' = \int_{-\infty}^{\infty}\left[f^{\rm QE}_{{\rm RFG},1}(\psi') + f^{\rm QE}_{{\rm RFG},2}(\psi')\right]d\psi' = 1. \tag{28}$$

If the normalization of the scaling function for negative values of ψ' is equal to

$$a = \int_{-\infty}^{0} d\psi' f^{\rm QE}_{{\rm RFG},1}(\psi') = \frac{2}{3}c_1, \tag{29}$$

then, to keep the total normalization [Eq. (28)], the normalization for positive ψ' has to be:

$$1-a = \int_{0}^{\infty} d\psi' f^{\rm QE}_{{\rm RFG},2}(\psi') = \frac{2}{3}c_1c_2. \tag{30}$$

From Eqs. (29) and (30) we get the relationship between c_2 and c_1:

$$c_2 = \frac{3}{2c_1} - 1. \tag{31}$$

In the RFG $c_1 = 3/4$ and, correspondingly, $c_2 = 1$. In the CDFM the QE scaling function will be:

$$f^{\rm QE}(\psi') = f^{\rm QE}_1(\psi') + f^{\rm QE}_2(\psi'), \tag{32}$$

where

$$f^{\rm QE}_1(\psi') \cong \int_0^{\alpha/k_F|\psi'|} dR|F(R)|^2c_1 \times\left[1-\left(\frac{k_FR|\psi'|}{\alpha}\right)^2\right], \qquad \psi' \leqslant 0, \tag{33}$$

$$f^{\rm QE}_2(\psi') \cong \int_0^{c_2\alpha/k_F|\psi'|} dR|F(R)|^2c_1 \times\left[1-\left(\frac{k_FR|\psi'|}{c_2\alpha}\right)^2\right], \qquad \psi' \geqslant 0. \tag{34}$$

In this approach, parametrizing the RFG scaling function by the coefficient c_1 we account for the experimental fact that $c_1 \neq 3/4$ and take this value in accordance with the empirical data. Then from the normalization [Eqs. (28)–(30)] we determine the corresponding value of c_2 using Eq. (31). As in Refs. [13,14], the CDFM scaling function is obtained [Eqs. (32)–(34)] by averaging the RFG scaling function. As an example, we give in Fig. 2 the CDFM QE scaling function for different values of c_1 (0.75, 0.72, 0.60, and 0.50) in comparison with the empirical data and the phenomenological fit. We also include for reference the scaling function obtained from calculations for (e, e') reaction based on the relativistic impulse approximation (RIA) with FSI described using the RMF potential (see Refs. [24,25] for details). In this way we simulate in a phenomenological way the role of the effects that violate the symmetry for positive values of ψ' of the QE scaling function, which in the RMF approximation are seen to be due to the FSI.

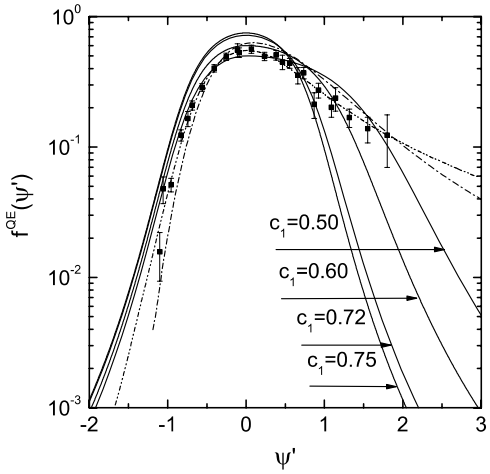

FIG. 2. The quasielastic scaling function $f^{\mathrm{QE}}(\psi')$ for ^{12}C calculated in CDFM in comparison with the experimental data (black squares) [23]. The CDFM results for different values of c_1 are presented by solid lines. Also shown for comparison is the phenomenological curve that fits the data (dash-two dots), as well as the curve (dash-dot line) corresponding to the result for (e, e') obtained within the relativistic impulse approximation and FSI using the relativistic mean field (see Refs. [24,25]).

B. QE scaling function in the LFD method

In this subsection we obtain the QE scaling function on the basis of calculations of nucleon momentum distribution [using Eqs. (5)–(7) or Eq. (13)] obtained within a modification of the approach from Ref. [44]. The latter is based on the momentum distribution in the deuteron from the LFD method (e.g., Refs. [45,46] and references therein). Using the natural-orbital representation of the one-body density matrix [55], $n(k)$ was written as a sum of contributions from hole states $[n^h(k)]$ and particle states $[n^p(k)]$ (see also Ref. [14])

$$n_A(k) = N_A[n^h(k) + n^p(k)]. \tag{35}$$

In Eq. (35)

$$n^h(k) = C(k) \sum_{nlj}^{\text{F.L.}} 2(2j+1)\lambda_{nlj}|R_{nlj}(k)|^2, \tag{36}$$

where F.L. denotes the Fermi level, and

$$C(k) = \frac{m_N}{(2\pi)^3\sqrt{k^2+m_N^2}}, \tag{37}$$

m_N being the nucleon mass. To a good approximation for the hole states, the natural occupation numbers λ_{nlj} are close to unity in Ref. [44] and the natural orbitals $R_{nlj}(k)$ are replaced by single-particle wave functions from the self-consistent mean-field approximation. In Ref. [44] Woods-Saxon single-particle wave functions were used for protons and neutrons. N_A is the normalization factor. Concerning the particle-state $[n^p(k)]$ contribution in Eq. (35), we used in Refs. [44] and [14] the well-known facts that (i) the high-momentum components of $n(k)$ caused by short-range and tensor correlations are almost completely determined by the contributions of the particle-state natural orbitals (e.g., Ref. [56]) and (ii) the high-momentum tails of $n_A(k)/A$ are approximately equal for all nuclei and are a rescaled version of the nucleon momentum distribution in the deuteron $n_d(k)$ [9],

$$n_A(k) \simeq \alpha_A n_d(k), \tag{38}$$

where α_A is a constant. These facts made it possible to assume in Refs. [44] and [14] that $n^{\mathrm{p}}(k)$ is related to the high-momentum components $n_5(k)$ of the deuteron, that is,

$$n^p(k) = \frac{A}{2} n_5(k). \tag{39}$$

In Eq. (39) $n_5(k)$ is expressed by an angle-averaged function [44] as

$$n_5(k) = C(k)\overline{(1-z^2)f_5^2(k)}. \tag{40}$$

In Eq. (40) $z = \cos(\widehat{\vec{k},\vec{n}})$, $\vec{n}$ being a unit vector along the three vector $(\vec{\omega})$ component of the four-vector ω that determines the position of the light-front surface [45,46]. The function $f_5(k)$ is one of the six scalar functions $f_{1-6}(k^2, \vec{n}\cdot\vec{k})$ that are the components of the deuteron total wave function $\Psi(\vec{k},\vec{n})$. It was shown [45] that f_5 largely exceeds other f components for $k \geqslant 2.0$–2.5 fm^{-1} and is the main contribution to the high-momentum component of $n_d(k)$, incorporating the main part of the short-range properties of the nucleon-nucleon interaction.

It was shown in Fig. 2 of Ref. [14] that the calculated LFD $n(k)$s are in good agreement with the "y-scaling data" for ^{4}He, ^{12}C, and ^{56}Fe from Ref. [5] and also with the y_{CW} analysis [7,8] up to $k \lesssim 2.8$ fm^{-1}. For larger k the momentum distributions from LFD exceeds that obtained from y_{CW} analysis. We should note also that the calculated scaling function $f^{\mathrm{QE}}(\psi')$ using the approximate relationship (see Eq. (75) and Fig. 4 of Ref. [14])

$$f^{\mathrm{QE}}(\psi') \simeq 3\pi \int_{|y|}^{\infty} d\bar{k}_F\, n(\bar{k}_F)\bar{k}_F{}^2,$$
$$|y| = \frac{1-\sqrt{1-4ck_F|\psi'|}}{2c}, \quad c \equiv \frac{\sqrt{1+m_N^2/q^2}}{2m_N}, \tag{41}$$

for ^{56}Fe at $q = 1000$ MeV/c is in agreement with the data for $-0.5 \lesssim \psi' \leqslant 0$, whereas in the region $-1.1 \leqslant \psi' \leqslant -0.5$ it shows a dip in the interval $-0.9 \leqslant \psi' \leqslant -0.6$. This difference is due to the particular form of $n(k)$ from LFD shown in Fig. 2 of Ref. [14] (a dip around $k \approx 1.7$ fm^{-1} and a very high-momentum tail at $k \gtrsim 2.8$ fm^{-1}). This result showed that the assumption (39) for the particle-state contribution is a rather rough one. In this article we consider a modification of the approach in which we include partially in the particle-state part $n^p(k)$ not only $n_5(k)$ but also $n_2(k)$, which is related to the angle-averaged function $f_2(k)$:

$$n_2(k) = C(k)\overline{f_2^2(k)}. \tag{42}$$

Then the particle-state part can be written in the form

$$n^p(k) = \beta[n_2(k) + n_5(k)], \tag{43}$$

where β is a parameter. Then the LFD nucleon momentum distribution for the nucleus with A nucleons will be:

$$n_{\mathrm{LFD}}(k) = N_A\{n^h(k) + \beta[n_2(k) + n_5(k)]\}, \tag{44}$$

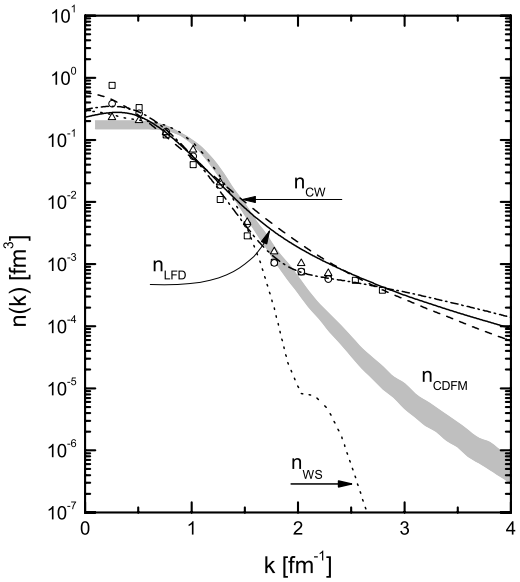

FIG. 3. The nucleon momentum distribution $n(k)$. (Gray area) CDFM combined results for ^{4}He, ^{12}C, ^{27}Al, ^{56}Fe, and ^{197}Au. (Solid line) Result of the present work for ^{12}C using the modified LFD approach with $\beta = 0.80$. (Dashed line) $y_{\rm CW}$-scaling result [7,8]. (Dash-dotted line) Result of LFD for ^{12}C from Ref. [44]. (Dotted line) Mean-field result using Wood-Saxon single-particle wave functions for ^{56}Fe. Open squares, circles, and triangles are y-scaling data [5] for ^{4}He, ^{12}C, and ^{56}Fe, respectively. The normalization is $\int n(k)d^3\mathbf{k} = 1$.

with $n^h(k)$ from Eq. (36) and

$$N_A = \left(4\pi \int_0^\infty dq\, q^2 \left\{ \sum_{nlj}^{\rm F.L.} 2(2j+1)\lambda_{nlj} C(q) |R_{nlj}(q)|^2 + \beta[n_2(q) + n_5(q)] \right\}\right)^{-1}. \quad (45)$$

In Fig. 3 we present the nucleon momentum distribution for ^{12}C calculated within the LFD method using Eqs. (35)–(37), (40), and (42)–(45) with the parameter value $\beta = 0.80$. It is compared with the band of CDFM momentum distributions for ^{4}He, ^{12}C, ^{27}Al, ^{56}Fe, and ^{197}Au (gray area), with $n_{\rm CW}(k)$ from the $y_{\rm CW}$ analysis [7,8] and with the y-scaling data [5] for ^{4}He, ^{12}C, and ^{56}Fe. It can be seen that up to $k \simeq 2.8$ fm^{-1} $n_{\rm LFD}$ curve is close to the results of Refs. [5,7,8]. For the region $1 \leqslant k \leqslant 2.5$ fm^{-1} it is between them and for $k \geqslant 2.8$ fm^{-1} it is close to $n_{\rm CW}(k)$, in contrast to our previous results in Fig. 2 of Ref. [14] (see also Ref. [44]), which were based on Eq. (39) and which are also shown for comparison in Fig. 3. This behavior of $n_{\rm LFD}(k)$ reflects in the result of the calculation of the QE scaling function using Eq. (41) given in Fig. 4. It can be seen that both momentum distributions $n_{\rm CW}$ [7] and $n_{\rm LFD}(k)$ [Eq. (44)] give a good agreement with the experimental data for the QE scaling function at least up to $\psi' \simeq -1.2$. This result is an improvement of that for LFD shown in Fig. 4 of Ref. [14], where only the contribution n_5 was used in the calculation of $n^p(k)$ (39) and $n_{\rm LFD}(k)$.

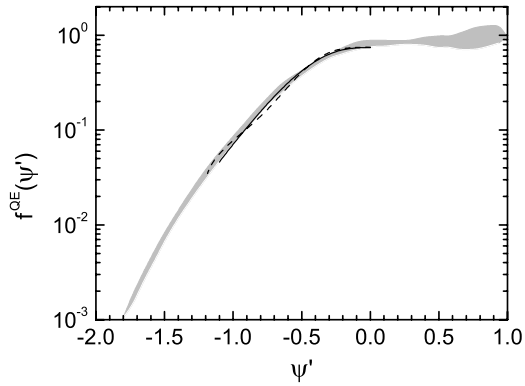

FIG. 4. The quasielastic scaling function $f^{\rm QE}(\psi')$ calculated using Eq. (41) at $q = 1000$ MeV/c with $n_{\rm CW}(k)$ from the $y_{\rm CW}$-scaling analysis [7,8] for ^{56}Fe (solid line) and $n_{\rm LFD}(k)$ from the modified LFD approach [Eq. (44)] for ^{12}C (dashed line).

III. SCALING FUNCTION IN THE QUASIELASTIC DELTA REGION

In this section we extend our analysis within both CDFM and LFD to the Δ-peak region, which is not too far above the QE peak region and is the main contribution to the inelastic scattering. Dividing the cross section by the appropriate single-nucleon cross section, now for $N \to \Delta$ transition, and displaying the results versus a new scaling variable (ψ'_Δ) (in which the kinematics of resonance electroproduction is accounted for) it is obtained in Ref. [23] that the results scale quite well. This is considered as an indication that the procedure has identified the dominant contributions not only in the QE region, but also in the Δ region.

The shifted dimensionless scaling variable in the Δ-region ψ'_Δ is introduced (see, e.g., Ref. [23]) by the expression:

$$\psi'_\Delta \equiv \left[\frac{1}{\xi_F}\left(\kappa\sqrt{{\rho'_\Delta}^2 + 1/\tau'} - \lambda'\rho'_\Delta - 1\right)\right]^{1/2} \times \begin{cases} +1, & \lambda' \geqslant \lambda'^0_\Delta \\ -1, & \lambda' \leqslant \lambda'^0_\Delta \end{cases}, \quad (46)$$

where

$$\xi_F \equiv \sqrt{1+\eta_F^2} - 1, \qquad \eta_F \equiv \frac{k_F}{m_N}, \quad (47)$$

$$\lambda' = \lambda - \frac{E_{\rm shift}}{2m_N}, \qquad \tau' = \kappa^2 - \lambda'^2, \quad (48)$$

$$\lambda = \frac{\omega}{2m_N}, \qquad \kappa = \frac{q}{2m_N}, \qquad \tau = \kappa^2 - \lambda^2, \quad (49)$$

$$\lambda'^0_\Delta = \lambda^0_\Delta - \frac{E_{\rm shift}}{2m_N}, \qquad \lambda^0_\Delta = \frac{1}{2}\left(\sqrt{\mu_\Delta^2 + 4\kappa^2} - 1\right), \quad (50)$$

$$\mu_\Delta = m_\Delta/m_N, \quad (51)$$

$$\rho_\Delta = 1 + \frac{\beta_\Delta}{\tau}, \qquad \rho'_\Delta = 1 + \frac{\beta_\Delta}{\tau'}, \quad (52)$$

$$\beta_\Delta = \frac{1}{4}\left(\mu_\Delta^2 - 1\right). \quad (53)$$

The relativistic Fermi gas superscaling function in the Δ domain is given by Ref. [23]:

$$f^{\Delta}_{\rm RFG}(\psi'_{\Delta}) = \tfrac{3}{4}(1-\psi'^{\,2}_{\Delta})\Theta(1-\psi'^{\,2}_{\Delta}). \tag{54}$$

Following the CDFM application to the scaling phenomenon, the Δ-scaling function in the model will be:

$$f^{\Delta}(\psi'_{\Delta}) = \int_0^{\infty} dR\,|F_{\Delta}(R)|^2 f^{\Delta}_{\rm RFG}[\psi'_{\Delta}(R)]. \tag{55}$$

In Eq. (55):

$$\psi'^{\,2}_{\Delta}(R) = \frac{1}{\left[\sqrt{1+\frac{k_F^2(R)}{m_N^2}}-1\right]}\left(\kappa\sqrt{\rho'^{2}_{\Delta}+\frac{1}{\tau'}}-\lambda'\rho'_{\Delta}-1\right)$$
$$\equiv t(R)\cdot\psi'^{2}_{\Delta}, \tag{56}$$

where

$$t(R) \equiv \frac{\left(\sqrt{1+\frac{k_F^2}{m_N^2}}-1\right)}{\left(\sqrt{1+\frac{k_F^2(R)}{m_N^2}}-1\right)} \quad \text{and} \quad k_F(R) = \frac{\alpha}{R}. \tag{57}$$

In the CDFM k_F can be calculated using the density distribution [Eqs. (8) and (9) or (19) and (16)] or the momentum distribution [Eqs. (10) and (11) or (25) and (24)]. The weight function $|F_{\Delta}(R)|^2$ is related to the density distributions [Eqs. (2) or (16)]. In the equivalent form of the CDFM, the scaling function can be written in the form:

$$f^{\Delta}(\psi'_{\Delta}) = \int_0^{\infty} d\bar{k}_F\,|G_{\Delta}(\bar{k}_F)|^2 f^{\Delta}_{\rm RFG}[\psi'_{\Delta}(\bar{k}_F)], \tag{58}$$

where $G_{\Delta}(\bar{k}_F)$ is determined by means of the momentum distribution [Eqs. (6) or (24)] and

$$\psi'^{2}_{\Delta}(\bar{k}_F) \equiv \widetilde{t}(\bar{k}_F)\cdot\psi'^{2}_{\Delta} \tag{59}$$

with

$$\widetilde{t}(\bar{k}_F) \equiv \frac{\left(\sqrt{1+\frac{k_F^2}{m_N^2}}-1\right)}{\left(\sqrt{1+\frac{\bar{k}_F^2}{m_N^2}}-1\right)}. \tag{60}$$

Here we note that though the functional forms of $f^{\Delta}(\psi'_{\Delta})$ [Eq. (55)] and the weight function $|F_{\Delta}(R)|^2$ [Eqs. (2) or (16)] are like before, i.e., as in the case of the QE region, the parameters of the densities (e.g., the half-radius R_{Δ} and the diffuseness b_{Δ} when Fermi-type forms have been used) may be different from those (R and b) in the QE case. Along this line, we calculated first the scaling function $f^{\Delta}(\psi'_{\Delta})$ by means of Eqs. (55)–(57) using the Fermi-type density for ^{12}C. We found the values of R_{Δ} and b_{Δ} fitting the scaling data at the Δ peak extracted from the high-quality world data for inclusive electron scattering (given in Fig. 2 of Ref. [23]). Our results are presented in Fig. 5. As mentioned in the QE case, the empirical data require to use a value of the coefficient in the right-hand side of Eq. (54) for the RFG scaling functions $f^{\Delta}_{\rm RFG}(\psi'_{\Delta})$ different from 3/4. In our calculations in the Δ region we use the value 0.54. We found that reasonable agreement

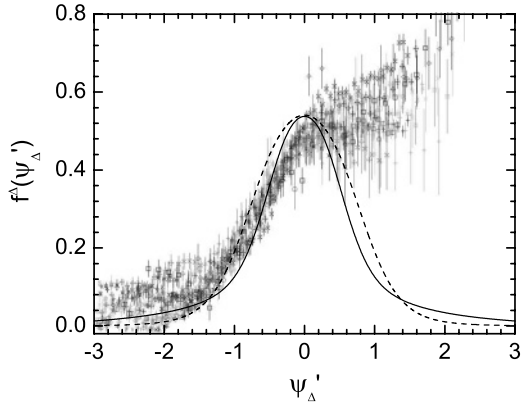

FIG. 5. The $f^{\Delta}(\psi'_{\Delta})$-scaling function for ^{12}C in the Δ region. (Dashed line) CDFM result (with $R_{\Delta} = 1.565$ fm, $b_{\Delta} = 0.420$ fm, $k_F = 1.20$ fm^{-1}). (Solid line) Result of modified LFD approach ($\beta = 0.80$, $k_F = 1.20$ fm^{-1}). The coefficient $c_1 = 0.54$ in both CDFM and LFD cases. Averaged experimental values of $f^{\Delta}(\psi'_{\Delta})$ are taken from Ref. [23].

with the data can be achieved using the parameter values $R_{\Delta} = 1.565$ fm and $b_{\Delta} = 0.420$ fm [the Fermi momentum value is taken to be $k_F = 1.20$ fm^{-1} and this choice leads to normalization to unity of $f^{\Delta}_{\rm RFG}(\psi'_{\Delta})$]. The value of R_{Δ} is smaller than that used in the description of the QE superscaling function for ^{12}C [13,14] ($R = 2.470$ fm), whereas the value of b_{Δ} is the same as b in the QE case. Second, we calculated $f^{\Delta}(\psi'_{\Delta})$ using Eqs. (58), (59), and (60). In Eq. (58) the weight function $|G_{\Delta}(\bar{k}_F)|^2$ was determined by means of Eq. (6) and the nucleon momentum distribution $n_{\rm LFD}$ [Eqs. (44) and (45)] calculated with the parameter value $\beta = 0.80$ (shown in Fig. 3). We note that the use of $n_{\rm LFD}(k)$ with this value of β gives simultaneously a reasonable agreement both with the results for the momentum distribution from the y-scaling data shown in Fig. 3, as well as with the QE scaling function shown in Fig. 4.

IV. SCALING FUNCTIONS AND INCLUSIVE LEPTON SCATTERING

A. Scaling functions and (e, e') reaction cross sections

In the beginning of this subsection we give some basic relationships concerning inclusive electron scattering from nuclei. An electron with four-momentum $k^{\mu} = (\epsilon, \mathbf{k})$ is scattered through an angle θ to four-momentum $k'^{\mu} = (\epsilon', \mathbf{k}')$. The four-momentum transfer is then

$$Q^{\mu} = (k-k')^{\mu} = (\omega, \mathbf{q}), \tag{61}$$

where $\omega = \epsilon - \epsilon'$, $q = |\mathbf{q}| = |\mathbf{k}-\mathbf{k}'|$ and

$$Q^2 = \omega^2 - q^2 \leqslant 0. \tag{62}$$

In the one-photon-exchange approximation, the double-differential cross section in the laboratory system can be

written in the form (e.g., Ref. [10]):

$$\frac{d^2\sigma}{d\Omega_{k'}d\epsilon'} = \sigma_M \left[\left(\frac{Q^2}{q^2} \right)^2 R_L(q,\omega) + \left(\frac{1}{2} \left| \frac{Q^2}{q^2} \right| + \tan^2 \frac{\theta}{2} \right) R_T(q,\omega) \right], \quad (63)$$

where

$$\sigma_M = \left[\frac{\alpha \cos(\theta/2)}{2\epsilon \sin^2(\theta/2)} \right]^2 \quad (64)$$

is the Mott cross section and α is the fine structure constant. In Eq. (63) R_L and R_T are the longitudinal and transverse response functions that contain all the information on the distribution of the nuclear electromagnetic charge and current densities, being projections (with respect to the momentum transfer direction) of the nuclear currents. They can be separated experimentally by plotting the cross section against $\tan^2(\theta/2)$ at fixed (q,ω) (the so-called Rosenbluth plot). These functions can be evaluated as components of the nuclear tensor $W_{\mu\nu}$. In Ref. [10] this tensor is computed in the framework of the RFG model, and $R_{L(T)}$ for the QE electron scattering are expressed by means of the RFG scaling function (Eq. (9) of Ref. [10]).

At leading order in the parameter k_F/m_N the QE responses have the form [23]:

$$R_L^{\rm QE}(\kappa,\lambda) = \Lambda_0 \frac{\kappa^2}{\tau}[(1+\tau)W_2(\tau) - W_1(\tau)] \times f_{\rm RFG}^{\rm QE}(\psi'), \quad (65)$$

$$R_T^{\rm QE}(\kappa,\lambda) = \Lambda_0 [2W_1(\tau)] \times f_{\rm RFG}^{\rm QE}(\psi'), \quad (66)$$

with

$$\Lambda_0 \equiv \frac{\mathcal{N}\xi_F}{m_N \kappa \eta_F^3}, \quad (67)$$

where $\mathcal{N} = Z$ or N and W_1, W_2 are the structure functions for elastic scattering that are linked to the Sachs form factors

$$(1+\tau)W_2(\tau) - W_1(\tau) = G_E^2(\tau), \quad (68)$$

$$2W_1(\tau) = 2\tau G_M^2(\tau). \quad (69)$$

In Refs. [23,57] the electroproduction of the Δ resonance is considered computing the nuclear tensor also within the RFG model and analytical expressions for the response functions are obtained. The latter contain the RFG Δ-peak scaling function (54) and read [57]:

$$R_L(\kappa,\lambda) = \frac{3\mathcal{N}\xi_F}{2m_N\eta_F^3\kappa}\frac{\kappa^2}{\tau}[(1+\tau\rho^2)w_2(\tau) - w_1(\tau) + w_2(\tau)D(\kappa,\lambda)] \times f_{\rm RFG}^{\Delta}(\psi'_\Delta), \quad (70)$$

$$R_T(\kappa,\lambda) = \frac{3\mathcal{N}\xi_F}{2m_N\eta_F^3\kappa}[2w_1(\tau) + w_2(\tau)D(\kappa,\lambda)] f_{\rm RFG}^{\Delta}(\psi'_\Delta), \quad (71)$$

where $\mathcal{N} = Z$ or N,

$$D(\kappa,\lambda) \equiv \frac{\tau}{\kappa^2}\left[(\lambda\rho+1)^2 + (\lambda\rho+1)(1+\psi_\Delta'^2)\xi_F + \frac{1}{3}(1+\psi_\Delta'^2+\psi_\Delta'^4)\xi_F^2\right] - (1+\tau\rho^2). \quad (72)$$

The single-baryon structure functions can be expressed by means of the electric (G_E), magnetic (G_M), and Coulomb (G_C) Δ form factors [57]:

$$w_1(\tau) = \tfrac{1}{2}(\mu_\Delta+1)^2(2\tau\rho+1-\mu_\Delta)\left(G_M^2 + 3G_E^2\right), \quad (73)$$

$$w_2(\tau) = \frac{1}{2}(\mu_\Delta+1)^2\frac{2\tau\rho+1-\mu_\Delta}{1+\tau\rho^2} \times \left(G_M^2 + 3G_E^2 + 4\frac{\tau}{\mu_\Delta^2}G_C^2\right). \quad (74)$$

These form factors are parametrized as follows [57]:

$$G_M(Q^2) = 2.97 f(Q^2), \quad (75)$$

$$G_E(Q^2) = -0.03 f(Q^2), \quad (76)$$

$$G_C(Q^2) = -0.15 G_M(Q^2), \quad (77)$$

where

$$f(Q^2) = G_E^P(Q^2)\frac{1}{\left[1 - \frac{Q^2}{3.5({\rm GeV}/c)^2}\right]^{1/2}} \quad (78)$$

with

$$G_E^P = \frac{1}{(1+4.97\tau)^2} \quad (79)$$

being the Galster parametrization [58] of the electric form factor.

In the CDFM the longitudinal and transverse response functions can be obtained by averaging the RFG response functions in the QE region [Eqs. (65) and (66)] and Δ region [Eqs. (70) and (71)] by means of the weight functions in r-space $|F(R)|^2$ and k-space $|G(\bar{k}_F)|^2$, similarly as in the case of the QE and Δ-scaling functions [Eqs. (1), (5), (15), (23) and (55), (58), respectively]. As a result, accounting for the different behavior of the RFG scaling functions and terms containing $\eta_F(R) = k_F(R)/m_N$ as functions of R or $\bar{k}_F = \alpha/R$ in Eqs. (65), (66), (70), and (71), the CDFM response functions $R_{L(T)}$ in QE and Δ regions have approximately the same forms as in the equations just mentioned, in which, however, the RFG scaling functions are changed by the CDFM scaling functions obtained in Secs. II and III.

In Figs. 6–15 we give results of calculations within the CDFM of inclusive electron scattering on ^{12}C at different incident energies and angles. The QE contribution is calculated using the Fermi-type density distribution of ^{12}C with the same values of the parameters as in Refs. [13,14]: $R = 2.47$ fm and $b = 0.42$ fm (which lead to a charge rms radius equal to the experimental one) and Fermi momentum $k_F = 1.156$ fm^{-1}. The Δ contribution is calculated using the necessary changes of the parameter values of the Fermi-type density (used in Fig. 5): $R_\Delta = 1.565$ fm, $b_\Delta = 0.42$ fm, and $k_F = 1.20$ fm^{-1}.

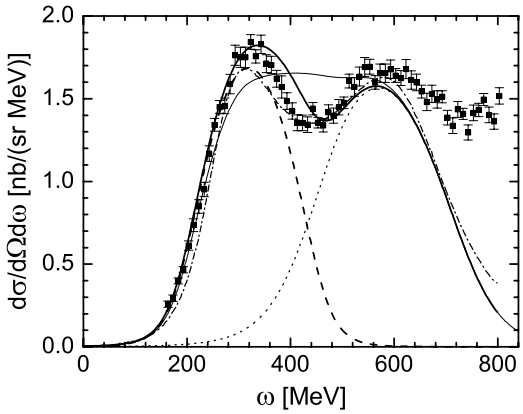

FIG. 6. Inclusive electron scattering on ^{12}C at $\epsilon = 1299$ MeV and $\theta = 37.5^\circ$ ($q^{\rm QE}_{\rm exp} = 792$ MeV/$c > 2k_F$). The results obtained using $c_1^{\rm QE} = 0.72$ in the CDFM scaling function for the QE cross section and the total result are given by dashed and thick solid lines, respectively. (Dotted line) Using CDFM Δ-scaling function; (thin solid line) total CDFM result with $c_1^{\rm QE} = 0.63$. (Dash-dotted line) Result of ERFG method [19,23]. The experimental data are taken from Ref. [59].

The coefficient c_1 used in the Δ-region scaling function is fixed to be equal to 0.54 so that the maximum of the scaling function to be in agreement with the data. The scaling function $f^{\Delta}(\psi'_{\Delta})$ is symmetric, its maximum is chosen to be 0.54 (but not 0.75) and it is normalized to unity by means of the fixed value of $k_F = 1.20\,{\rm fm}^{-1}$. The inclusive electron-^{12}C scattering cross sections shown in Figs. 6–15 are the sum of the QE and Δ contribution. The results of the CDFM calculations are presented for two values of the coefficient c_1 in the QE case (noted further by $c_1^{\rm QE}$), namely for $c_1^{\rm QE} \simeq 0.72$ and $c_1^{\rm QE} = 0.63$. This is related to two types of experimental data. In the first one the transferred momentum in the position of the maximum of the QE peak extracted from data ($\omega^{\rm QE}_{\rm exp}$) is $q^{\rm QE}_{\rm exp} \geqslant 450$ MeV/c

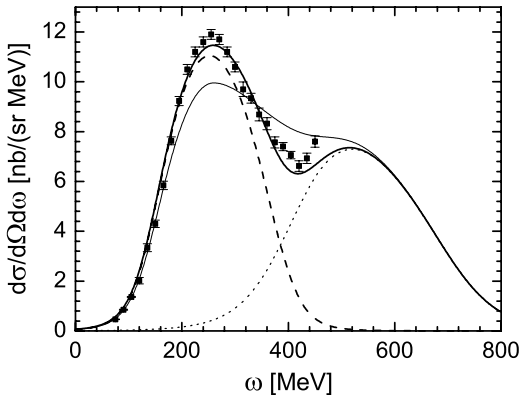

FIG. 7. Inclusive electron scattering on ^{12}C at $\epsilon = 2020$ MeV and $\theta = 20.02^\circ$ ($q^{\rm QE}_{\rm exp} = 703$ MeV/$c > 2k_F$). The results obtained using $c_1^{\rm QE} = 0.73$ in the CDFM scaling function for the QE cross section and the total result are given by dashed and thick solid lines, respectively. (Dotted line) Using CDFM Δ-scaling function. (Thin solid line) Total CDFM result with $c_1^{\rm QE} = 0.63$. The experimental data are taken from Ref. [60].

$\approx 2k_F$, roughly corresponding to the domain where scaling is fulfilled [19,23]. Such cases are presented in Figs. 6–12. In these cases we found by fitting to the maximum of the QE peak the value of $c_1^{\rm QE}$ to be 0.72–0.73, i.e., it is not the same as in the RFG model case (case of symmetry of the RFG and of the CDFM scaling functions with $c_1^{\rm QE} = 0.75$), but is slightly lower. This leads to a weak asymmetry of the CDFM scaling function for cases in which $q^{\rm QE}_{\rm exp} \geqslant 450$ MeV/c. In the second type of experimental data $q^{\rm QE}_{\rm exp}$ is not in the scaling region ($q^{\rm QE}_{\rm exp} < 450$ MeV/c). Such cases are given in Figs. 13–15. For them we found by fitting to the maximum of the QE peak extracted from data the value of $c_1^{\rm QE}$ to be 0.63. For these cases the CDFM scaling function is definitely asymmetric. So, the results in Figs. 6–15 are presented for both almost symmetric ($c_1^{\rm QE} \simeq 0.72$) and asymmetric ($c_1^{\rm QE} = 0.63$) CDFM scaling functions. One can see that the results for the almost symmetric CDFM scaling function agree with the electron data in the region close to the QE peak in cases where $q^{\rm QE}_{\rm exp} \geqslant 450$ MeV/c and overestimate the data for cases where approximately $q^{\rm QE}_{\rm exp} < 450$ MeV/c. The results with asymmetric CDFM scaling function agree with the data in cases where $q^{\rm QE}_{\rm exp} < 450$ MeV/c and underestimate the data in cases where $q^{\rm QE}_{\rm exp} \geqslant 450$ MeV/c. Here we emphasize that, in our opinion, the usage of an asymmetric CDFM scaling function is preferable, though the results in some cases can underestimate the empirical data, because other additional effects, apart from QE and Δ resonance (e.g., meson exchange currents effects) could give important contributions to the cross section for some specific kinematics and minor for others. A similar situation occurs for the results obtained within the RMF approach [25] particularly when the CC2 current operator is selected.

In Table I we list the energies, the angles, the values of $c_1^{\rm QE}$ obtained by fitting the magnitude of the QE peak, and the energy shifts in the QE and Δ case, as well as the approximate values of the transfer momentum $q^{\rm QE}_{\rm exp}$ in the position of the maximum of the QE peak ($\omega^{\rm QE}_{\rm exp}$) for different cases. The values of the energy shifts $\epsilon^{\rm QE(\Delta)}_{\rm shift}$ for the QE and Δ regions

TABLE I. Values of energies ϵ, angles θ, the coefficient $c_1^{\rm QE}$ obtained by fitting the magnitude of the QE peak, energy shifts $\epsilon^{\rm QE}_{\rm shift}$ and $\epsilon^{\Delta}_{\rm shift}$, and transferred momenta $q^{\rm QE}_{\rm exp}$ for the cases of inclusive electron-scattering cross sections considered. Energies are in MeV, angles are in degrees, and momenta are in MeV/c.

Figure	ϵ	θ	$c_1^{\rm QE}$	$\epsilon^{\rm QE}_{\rm shift}$	$\epsilon^{\Delta}_{\rm shift}$	$\approx q^{\rm QE}_{\rm exp}$
6	1299	37.5	0.72	30	30	792
7	2020	20.02	0.73	25	20	703
8	1108	37.5	0.73	30	30	675
9	620	60	0.73	20	0	552
10	2020	15.02	0.72	20	30	530
11	500	60	0.72	30	0	450
12	730	37.1	0.72	20	20	$442 \simeq 2k_F$
13	1650	13.5	0.63	20	30	390
14	1500	13.5	0.63	20	20	352
15	537	37.1	0.63	20	20	326

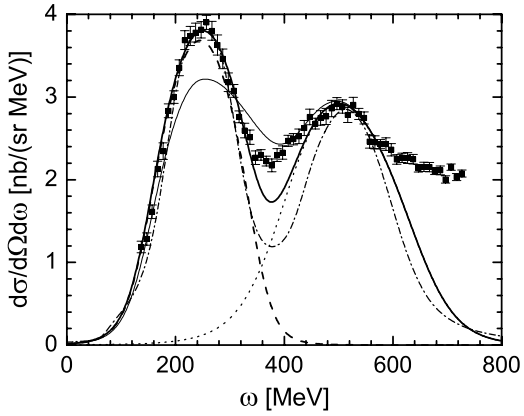

FIG. 8. The same as described in the legend to Fig. 7 for $\epsilon =$ 1108 MeV and $\theta = 37.5^\circ$ ($q_{\rm exp}^{\rm QE} = 675$ MeV/$c > 2k_F$). (Dot-dashed line) Using QE and Δ-scaling functions obtained in the LFD approach. The experimental data are taken from Ref. [59].

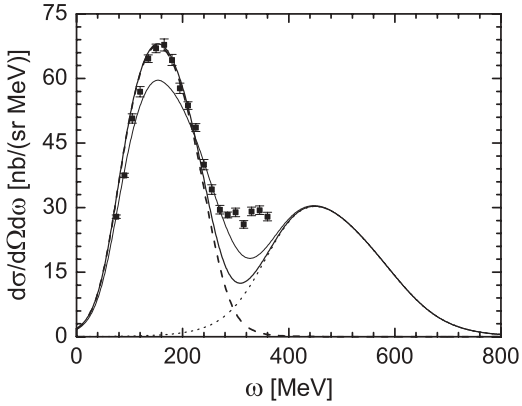

FIG. 10. The same as described in the legend to Fig. 6 for $\epsilon =$ 2020 MeV and $\theta = 15.02^\circ$ ($q_{\rm exp}^{\rm QE} = 530$ MeV/$c > 2k_F$) for the CDFM results. The experimental data are taken from Ref. [60].

are generally between 20 and 30 MeV. In the figures we also present the QE contribution (as well as the Δ contribution) for the value of $c_1^{\rm QE}$ that fits approximately the magnitude of the QE peak.

In Figs. 8 and 11 we present also the calculations of the electron cross sections using QE- and Δ-scaling functions obtained by using the nucleon momentum distributions obtained in the LFD approach (Sec. III) that give a reasonable agreement with the empirical electron scattering data. In Figs. 6 and 14 we also give for comparison the results of the cross sections obtained within the ERFG method [19,23]. In this method the response functions and differential cross sections are calculated using the scaling function fitted to the data.

It is interesting to note that for those kinematics where the overlap between the QE and Δ peaks is bigger (Figs. 6, 7, and 8), the asymmetric CDFM model ($c_1^{\rm QE} = 0.63$) gives rise to an excess of strength in the transition region. This makes a difference with the ERFG model (see Fig. 6), which fits nicely the data in that region. This discrepancy between the two models, asymmetric CDFM and ERFG, can be explained by noting the different behavior presented by the two scaling functions in the region of ψ' between 0.5 and 1.5, being the asymmetric CDFM one significantly larger.

Note that in the cases where the overlap between the QE and Δ peaks is weaker (Figs. 9–12), the asymmetric CDFM model, compared to the almost symmetric CDFM one, reproduces better the data in the transition region although, importantly, it underpredicts the maximum of the QE peak. Concerning results in Figs. 13–15 (it can be also applied to Figs. 11 and 12), one observes that both CDFM approaches do not reproduce the strength of data located in the region between the QE and Δ peaks. This is not the case for the ERFG model (see Fig. 14), which fits nicely the experiment for $\omega \geqslant 180$ MeV. This result is connected with the much bigger strength of the scaling function provided by the ERFG model for larger values of the scaling variable, $\psi' \geqslant 2$ (see Fig. 2).

From this whole analysis, one may conclude that the phenomenological procedure introduced in the CDFM model to get an asymmetric scaling function gives rise to an excess of

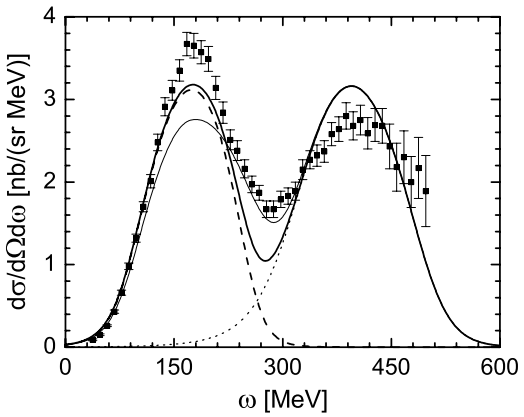

FIG. 9. The same as described in the legend to Fig. 7 for $\epsilon =$ 620 MeV and $\theta = 60^\circ$ ($q_{\rm exp}^{\rm QE} = 552$ MeV/$c > 2k_F$). The experimental data are taken from Ref. [61].

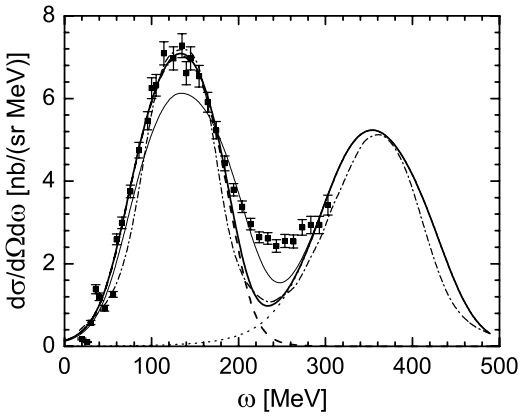

FIG. 11. The same as described in the legend to Fig. 6 for $\epsilon =$ 500 MeV and $\theta = 60^\circ$ ($q_{\rm exp}^{\rm QE} = 450$ MeV/$c \geqslant 2k_F$). Here the dot-dashed line shows the result using QE and Δ-scaling functions obtained in the LFD approach. The experimental data are taken from Ref. [62].

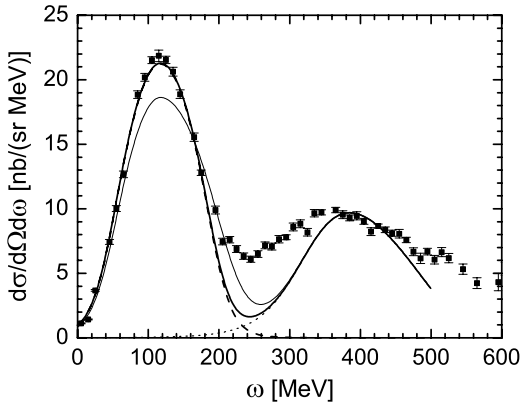

FIG. 12. The same as described in the legend to Fig. 6 for $\epsilon =$ 730 MeV and $\theta = 37.1^\circ$ ($q_{\rm exp}^{\rm QE} = 442$ MeV/$c \leqslant 2k_F$) for the CDFM results. The experimental data are taken from Ref. [63].

strength in the region $0.5 \leqslant \psi' \leqslant 1.5$, whereas the model lacks strength for larger ψ' values, $\psi' \geqslant 2$.

B. Scaling functions and charge-changing neutrino-nucleus reaction cross sections

In this subsection we present applications of the CDFM and LFD scaling functions to calculations of charge-changing neutrino-nucleus reaction cross sections. We follow the description of the formalism given in Ref. [23]. The charge-changing neutrino cross section in the target laboratory frame is given in the form

$$\left(\frac{d^2\sigma}{d\Omega dk'}\right)_\chi \equiv \sigma_0 \mathcal{F}_\chi^2, \tag{80}$$

where $\chi = +$ for neutrino-induced reactions (e.g., $\nu_\ell + n \to \ell^- + p$, where $\ell = e, \mu, \tau$) and $\chi = -$ for antineutrino-induced reactions (e.g., $\overline{\nu}_\ell + p \to \ell^+ + n$),

$$\sigma_0 \equiv \frac{(G\cos\theta_c)^2}{2\pi^2}(k'\cos\tilde{\theta}/2)^2, \tag{81}$$

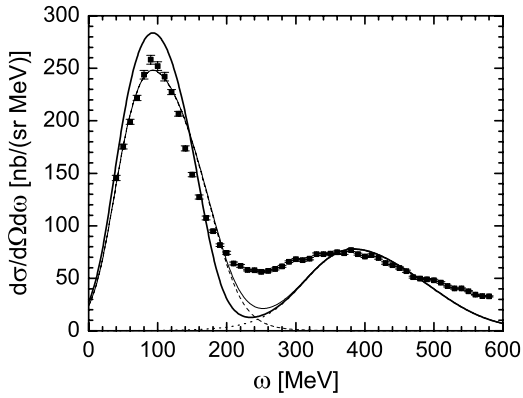

FIG. 13. The same as described in the legend to Fig. 6 for $\epsilon =$ 1650 MeV and $\theta = 13.5^\circ$ ($q_{\rm exp}^{\rm QE} = 390$ MeV/$c \leqslant 2k_F$) for the CDFM results. The experimental data are taken from Ref. [64].

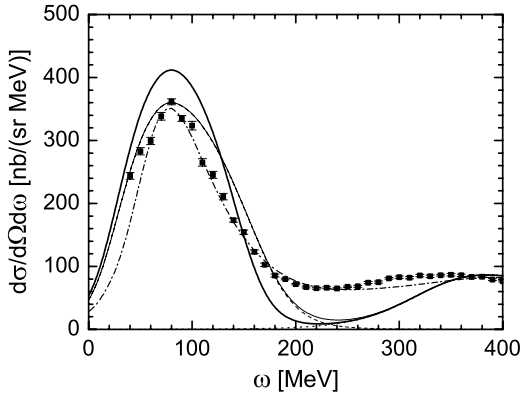

FIG. 14. The same as described in the legend to Fig. 6 for $\epsilon = 1500$ MeV and $\theta = 13.5^\circ$ ($q_{\rm exp}^{\rm QE} = 352$ MeV/$c \leqslant 2k_F$). The experimental data are taken from Ref. [64].

$G = 1.16639 \times 10^{-5}$ GeV^{-2} being the Fermi constant, θ_c being Cabibbo angle ($\cos\theta_c = 0.9741$),

$$\tan^2\tilde{\theta}/2 \equiv \frac{|Q|^2}{v_0}, \tag{82}$$

$$v_0 \equiv (\epsilon + \epsilon')^2 - q^2 = 4\epsilon\epsilon' - |Q|^2. \tag{83}$$

The quantity $\mathcal{F}_\chi^2$, which depends on the nuclear structure, is written in Ref. [23] as a generalized Rosenbluth decomposition having charge-charge, charge-longitudinal, longitudinal-longitudinal, and two types of transverse responses. The nuclear response functions are expressed in terms of the nuclear tensor $W^{\mu\nu}$ in both QE and Δ regions using its relationships with the RFG model scaling functions. Following Ref. [23], in the calculations of the neutrino-nucleus cross sections the Höhler parametrization 8.2 [65] of the form factors in the vector sector was used, whereas in the axial-vector sector the form factors given in Ref. [23] were used.

In our work, instead of the RFG scaling functions in the QE and Δ regions, we use those obtained in the CDFM and LFD approach (Secs. II and III). In Fig. 16 we give the results of calculations for cross sections of QE neutrino (ν_μ, μ^-) scattering [Figs. 16(a) and 16(c)–16(f)] on ^{12}C and

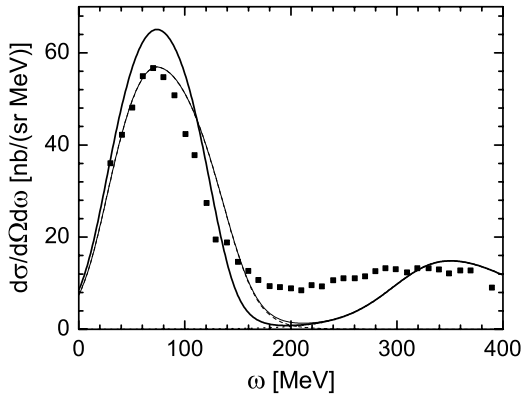

FIG. 15. The same as described in the legend to Fig. 6 for $\epsilon =$ 537 MeV and $\theta = 37.1^\circ$ ($q_{\rm exp}^{\rm QE} = 326$ MeV/$c \leqslant 2k_F$) for the CDFM results. The experimental data are taken from Ref. [63].

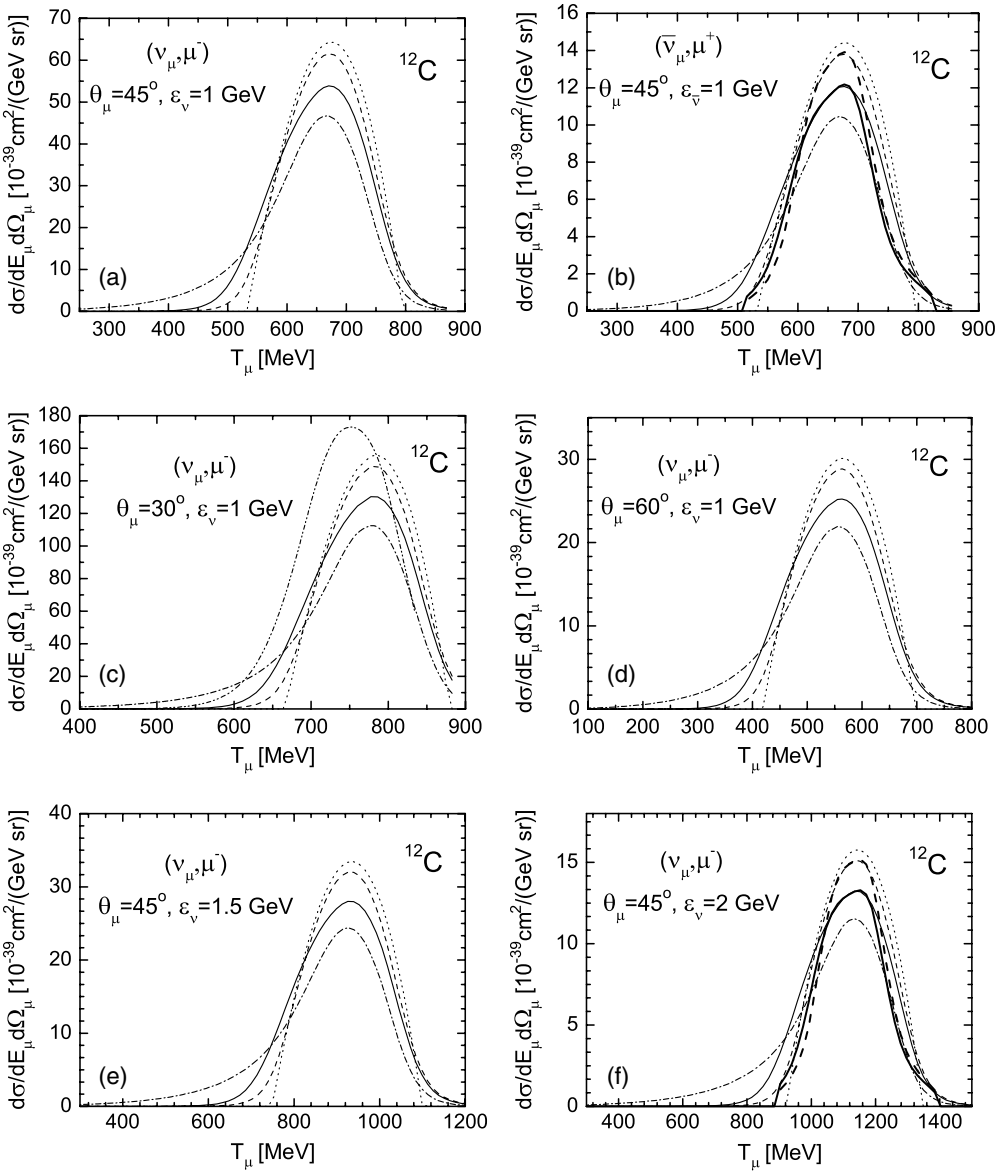

FIG. 16. The cross section of quasielastic charge-changing (ν_μ, μ^-) reaction [(a) and (c)–(f)] and of $(\overline{\nu}_\mu, \mu^+)$ reaction (b) on ^{12}C for $\epsilon = 1$, 1.5, and 2 GeV using QE scaling functions in CDFM [(thin solid line) with $c_1 = 0.63$; (thin dashed line) with $c_1 = 0.72$)]. The results using QE scaling functions in LFD [(thick solid line) with $c_1 = 0.63$; (thick dashed line) with $c_1 = 0.72$] are presented in (b) and (f). The RFG model result and ERFG result [19,23] are shown by dotted and dash-dotted lines, respectively.

also antineutrino $(\overline{\nu}_\mu, \mu^+)$ scattering [Fig. 16(b)] for energies of neutrino $\epsilon_\nu = 1$, 1.5, and 2 GeV and of antineutrino $\epsilon_{\overline{\nu}} =$ 1 GeV. The presented cross sections are functions of muon kinetic energy. The energy shift is equal to 20 MeV. The calculations of the neutrino-nucleus cross sections in the Δ region will be a subject of a future work.

We give the results of our calculations using the CDFM scaling function that is almost symmetric (with $c_1 = 0.72$), as well as those of the asymmetric CDFM scaling function (with $c_1 = 0.63$). These values of c_1 correspond to the cases of inclusive electron scattering considered. As can be seen the results obtained by using the almost symmetric CDFM scaling function are close to the RFG model results. However, the results obtained with the use of asymmetric CDFM and LFD scaling functions are quite different from those in the RFG model but are close to the predictions of the ERFG model [19,23]. The basic difference from the ERFG model result is observed in the tail extended to small muon energy values, where the ERFG model gives more strength.

V. CONCLUSIONS

The results of the present work can be summarized as follows:

(i) In Ref. [14] we extended the CDFM description of the quasielastic ψ'-scaling function from Ref. [13] by expressing it explicitly and equivalently by means of both density and nucleon momentum distributions. In Refs. [13,14] our results

on $f^{\mathrm{QE}}(\psi')$ were obtained on the basis of the experimental data on the charge densities for a wide range of nuclei. In the present work we extended our approach to consider the scaling function $f^{\mathrm{QE}}(\psi')$ for medium and heavy nuclei with $Z \neq N$ for which the proton and neutron densities are not similar. In this case $f^{\mathrm{QE}}(\psi')$ is a sum of the proton and neutron scaling functions calculated by means of the proton and neutron densities obtained from nonrelativistic self-consistent mean-field calculations. This concerns calculations, as examples, of nuclei like ^{197}Au, ^{82}Kr, as well as ^{62}Ni and ^{118}Sn [15]. The comparison with the data from Refs. [11,12] shows superscaling for negative values of the QE ψ', including $\psi' < -1$, whereas in the RFG model $f(\psi') = 0$ for $\psi' \leqslant -1$ (see Fig. 1).

(ii) We introduce the asymmetry in the CDFM QE scaling function using the fact that the maximum value of $f(\psi')$ in RFG model is 3/4, whereas the empirical scaling function reaches values smaller than 0.6. In relation with this and the normalization, we parametrize the RFG scaling function for $\psi' \geqslant 0$, thus simulating the role of all the effects that lead to asymmetry and imposing this on the CDFM QE scaling function. In this way, simulating phenomenologically the effects that violate the symmetry of $f^{\mathrm{QE}}(\psi')$ for $\psi' \geqslant 0$, including the role of the FSI, one can obtain in the CDFM a reasonable agreement of $f^{\mathrm{QE}}(\psi')$ with the empirical data also for positive values of ψ' (Fig. 2).

(iii) We obtain the QE scaling function also on the basis of calculations of nucleon momentum distribution $n(k)$ within an approach based on the LFD method [44–46] that improves that used in Ref. [14]. Here we include in the particle-state part of $n(k)$ not only a contribution of the function f_5 (as in Refs. [44] and [14]) but also a contribution of the function f_2. f_5 and f_2 are two of the six scalar components of the deuteron total wave function in the LFD [45,46] and are the main contributions to the tail of $n_d(k)$. It can be seen in Fig. 3 the reasonable agreement of $n(k)$ in LFD with the y_{CW}-scaling data [7,8]. This result made it possible to obtain a good description of the experimental QE scaling function (Fig. 4) at least up to $\psi' \simeq -1.2$.

(iv) We extend our analysis within the CDFM and LFD to the Δ-peak region, which is the main contribution to the inelastic scattering. Here we emphasize that reasonable agreement with the experimental data (Fig. 5) was obtained using the empirical value of the coefficient in front of the RFG scaling function (0.54 instead of 0.75) in both CDFM and LFD. Also, the parameter R_Δ used in the Fermi-type density for ^{12}C [necessary to calculate the weight function $|F_\Delta(R)|^2$ and thus the scaling function $f^{\Delta}(\psi'_\Delta)$] has a smaller value (1.565 fm) than that ($R = 2.42$ fm) in the QE case, whereas the value of the diffuseness parameter b_Δ remains the same as b in the QE case. We note that the use of $n_{\mathrm{LFD}}(k)$ with the same values of β and of k_F ($\beta = 0.80$, $k_F = 1.20$ fm^{-1}) gives a reasonable agreement with results for both QE and Δ-region scaling functions (Figs. 4 and 5).

(v) The QE and Δ-region scaling functions obtained in the CDFM and in the LFD approach are applied to description of experimental data on differential cross sections of inclusive electron scattering by ^{12}C at large energies and transferred momenta (Figs. 6–15). The CDFM results are presented for both almost symmetric ($c_1^{\mathrm{QE}} \simeq 0.72$) and asymmetric ($c_1^{\mathrm{QE}} = 0.63$) scaling functions. We observe that there are two regions of the value of $q_{\mathrm{exp}}^{\mathrm{QE}}$ in different experiments at which the above mentioned (almost symmetric and asymmetric) scaling functions work better. The almost symmetric scaling function leads to results in agreement with the data in the region of the QE peak in cases when the transferred momentum ($q_{\mathrm{exp}}^{\mathrm{QE}}$) in the position of maximum of the QE peak ($\omega_{\mathrm{exp}}^{\mathrm{QE}}$) is in the scaling region ($q_{\mathrm{exp}}^{\mathrm{QE}} \geqslant 450$ MeV/$c \approx 2k_F$), whereas the data are overestimated in cases where $q_{\mathrm{exp}}^{\mathrm{QE}} < 450$ MeV/c. The results obtained when asymmetric scaling function ($c_1^{\mathrm{QE}} = 0.63$) is used agree with the data in cases when $q_{\mathrm{exp}}^{\mathrm{QE}} < 450$ MeV/c and underestimate them when $q_{\mathrm{exp}}^{\mathrm{QE}} \geqslant 450$ MeV/c in the region close to the QE peak, but differences emerge in the transition region. In our opinion, the latter case is preferable because additional effects (apart from QE and Δ resonance), e.g., of the meson exchange currents could give additional important contributions to the inclusive electron cross sections for some specific kinematics and minor for others.

(vi) The CDFM and LFD scaling functions are applied to calculations of QE charge-changing neutrino-nuclei reaction cross sections. We present in Fig. 16 the predicted cross sections for the reactions (ν_μ, μ^-) and $(\overline{\nu}_\mu, \mu^+)$ on the ^{12}C nucleus for energies of the incident particles from 1 to 2 GeV. Our results are compared with those from the RFG model and from the ERFG model [19,23]. The results obtained by using the asymmetric CDFM scaling function are close to those of ERFG and are quite different from the RFG results, whereas the almost symmetric CDFM scaling function leads to cross sections that are similar to the results of the RFG model.

ACKNOWLEDGMENTS

Four of the authors (A.N.A., M.V.I., M.K.G., and M.B.B.) are grateful to C. Giusti and A. Meucci for the discussion. This work was partly supported by the Bulgarian National Science Foundation under contracts Φ-1416 and Φ-1501 and by funds provided by DGI of MCyT (Spain) under contracts FIS 2005-00640, BFM 2003-04147-C02-01, INTAS-03-54-6545, FPA 2005-04460, and FIS 2005-01105.

[1] G. B. West, Phys. Rep. **18**, 263 (1975).
[2] I. Sick, D. B. Day, and J. S. McCarthy, Phys. Rev. Lett. **45**, 871 (1980).
[3] D. B. Day, J. S. McCarthy, T. W. Donnelly, and I. Sick, Annu. Rev. Nucl. Part. Sci. **40**, 357 (1990).
[4] C. Ciofi degli Atti, E. Pace, and G. Salmè, Phys. Rev. C **36**, 1208 (1987).
[5] C. Ciofi degli Atti, E. Pace, and G. Salmè, Phys. Rev. C **43**, 1155 (1991).
[6] C. Ciofi degli Atti and S. Simula, Phys. Rev. C **53**, 1689 (1996).
[7] C. Ciofi degli Atti and G. B. West, nucl-th/9702009.
[8] C. Ciofi degli Atti and G. B. West, Phys. Lett. **B458**, 447 (1999).
[9] D. Faralli, C. Ciofi degli Atti, and G. B. West, in *Proceedings of the 2nd International Conference on Perspectives in Hadronic*

Physics, ICTP, Trieste, Italy, 1999, edited by S. Boffi, C. Ciofi degli Atti, and M. M. Giannini (World Scientific, Singapore, 2000), p. 75.
[10] W. M. Alberico, A. Molinari, T. W. Donnelly, E. L. Kronenberg, and J. W. Van Orden, Phys. Rev. C **38**, 1801 (1988).
[11] T. W. Donnelly and I. Sick, Phys. Rev. Lett. **82**, 3212 (1999).
[12] T. W. Donnelly and I. Sick, Phys. Rev. C **60**, 065502 (1999).
[13] A. N. Antonov, M. K. Gaidarov, D. N. Kadrev, M. V. Ivanov, E. Moya de Guerra, and J. M. Udias, Phys. Rev. C **69**, 044321 (2004).
[14] A. N. Antonov, M. K. Gaidarov, M. V. Ivanov, D. N. Kadrev, E. Moya de Guerra, P. Sarriguren, and J. M. Udias, Phys. Rev. C **71**, 014317 (2005).
[15] A. N. Antonov, M. V. Ivanov, M. K. Gaidarov, E. Moya de Guerra, P. Sarriguren, and J. M. Udias, Phys. Rev. C **73**, 047302 (2006).
[16] M. B. Barbaro, R. Cenni, A. De Pace, T. W. Donnelly, and A. Molinari, Nucl. Phys. **A643**, 137 (1998).
[17] C. Maieron, T. W. Donnelly, and I. Sick, Phys. Rev. C **65**, 025502 (2002).
[18] O. Benhar, D. Day, and I. Sick, nucl-ex/0603029.
[19] M. B. Barbaro, J. A. Caballero, T. W. Donnelly, and C. Maieron, Phys. Rev. C **69**, 035502 (2004).
[20] L. Alvarez-Ruso, M. B. Barbaro, T. W. Donnelly, and A. Molinari, Nucl. Phys. **A724**, 157 (2003).
[21] J. E. Amaro, M. B. Barbaro, J. A. Caballero, T. W. Donnelly, and A. Molinari, Nucl. Phys. **A697**, 388 (2002); **A723**, 181 (2003); Phys. Rep. **368**, 317 (2002).
[22] A. De Pace, M. Nardi, W. M. Alberico, T. W. Donnelly, and A. Molinari, Nucl. Phys. **A726**, 303 (2003); **A741**, 249 (2004).
[23] J. E. Amaro, M. B. Barbaro, J. A. Caballero, T. W. Donnelly, A. Molinari, and I. Sick, Phys. Rev. C **71**, 015501 (2005).
[24] J. A. Caballero, J. E. Amaro, M. B. Barbaro, T. W. Donnelly, C. Maieron, and J. M. Udias, Phys. Rev. Lett. **95**, 252502 (2005).
[25] J. A. Caballero, Phys. Rev. C **74**, 015502 (2006).
[26] Y. Fukuda *et al*. (The Super-Kamiokande Collaboration), Phys. Rev. Lett. **81**, 1562 (1998); M. H. Ahn *et al*. (K2K Collaboration), *ibid*. **90**, 041801 (2003); Q.-R. Ahmad *et al*. (SNO Collaboration), *ibid*. **87**, 071301 (2001); **89**, 011301 (2002); K. Eguchi *et al*. (KamLAND Collaboration), *ibid*. **90**, 021802 (2003); C. Athanassopoulos *et al*. (LSND Collaboration), *ibid*. **77**, 3082 (1996); **81**, 1774 (1998).
[27] A. Meucci, C. Giusti, and F. D. Pacati, Nucl. Phys. **A744**, 307 (2004).
[28] J. E. Amaro, M. B. Barbaro, J. A. Caballero, and T. W. Donnelly, Phys. Rev. C **73**, 035503 (2006).
[29] M. C. Martinez, P. Lava, N. Jachowicz, J. Ryckebusch, and J. M. Udias, Phys. Rev. C **73**, 024607 (2006).
[30] M. B. Barbaro, Nucl. Phys. B., Proc. Suppl. **159**, 186 (2006); nucl-th/0602011.
[31] J. Nieves, M. Valverde, and M. J. Vicente-Vacas, Nucl. Phys. B., Proc. Suppl. **155**, 263 (2006); nucl-th/0510010.
[32] M. B. Barbaro, J. E. Amaro, J. A. Caballero, T. W. Donnelly, A. Molinari, and I. Sick, nucl-th/0509022; Nucl. Phys. B., Proc. Suppl. **155**, 257 (2006).
[33] C. Maieron, M. C. Martinez, J. A. Caballero, and J. M. Udias, Phys. Rev. C **68**, 048501 (2003).
[34] A. Meucci, C. Giusti, and F. D. Pacati, Nucl. Phys. **A739**, 277 (2004); **A773**, 250 (2006).
[35] O. Benhar, Nucl. Phys. B-Proc. Suppl. **139**, 15 (2005); nucl-th/0408045.
[36] O. Benhar and N. Farina, Nucl. Phys. B., Proc. Suppl. **139**, 230 (2005); nucl-th/0407106.
[37] O. Benhar, N. Farina, H. Nakamura, M. Sakuda, and R. Seki, Nucl. Phys. B., Proc. Suppl. **155**, 254 (2006); hep-ph/0510259; Phys. Rev. D **72**, 053005 (2005).
[38] G. Co', Nucl. Phys. B., Proc. Suppl. **159**, 192 (2006); nucl-th/0601034.
[39] A. Botrugno and G. Co', Nucl. Phys. **A761**, 200 (2005).
[40] A. N. Antonov, P. E. Hodgson, and I. Zh. Petkov, *Nucleon Momentum and Density Distributions in Nuclei* (Clarendon Press, Oxford, 1988).
[41] A. N. Antonov, P. E. Hodgson, and I. Zh. Petkov, *Nucleon Correlations in Nuclei* (Springer-Verlag, New York, 1993).
[42] A. N. Antonov, V. A. Nikolaev, and I. Zh. Petkov, Bulg. J. Phys. **6**, 151 (1979); Z. Phys. A **297**, 257 (1980); **304**, 239 (1982); Nuovo Cimento A **86**, 23 (1985).
[43] A. N. Antonov, E. N. Nikolov, I. Zh. Petkov, C. V. Christov, and P. E. Hodgson, Nuovo Cimento A **102**, 1701 (1989); A. N. Antonov, D. N. Kadrev, and P. E. Hodgson, Phys. Rev. C **50**, 164 (1994).
[44] A. N. Antonov, M. K. Gaidarov, M. V. Ivanov, D. N. Kadrev, G. Z. Krumova, P. E. Hodgson, and H. V. von Geramb, Phys. Rev. C **65**, 024306 (2002).
[45] J. Carbonell and V. A. Karmanov, Nucl. Phys. **A581**, 625 (1995).
[46] J. Carbonell, B. Desplanques, V. A. Karmanov, and J.-F. Mathiot, Phys. Rep. **300**, 215 (1998).
[47] J. J. Griffin and J. A. Wheeler, Phys. Rev. **108**, 311 (1957).
[48] J. D. Patterson and R. J. Peterson, Nucl. Phys. **A717**, 235 (2003).
[49] E. Moya de Guerra, P. Sarriguren, J. A. Caballero, M. Casas, and D. W. L. Sprung, Nucl. Phys. **A529**, 68 (1991).
[50] D. Vautherin, Phys. Rev. C **7**, 296 (1973).
[51] J. Jourdan, Nucl. Phys. **A603**, 117 (1996).
[52] H. Kim, J. Pieckarewicz, and C. J. Horowitz, Phys. Rev. C **51**, 2739 (1995); H. Kim, S. Schramm, and C. J. Horowitz, *ibid*. **53**, 2468 (1996).
[53] W. M. Alberico *et al*., Nucl. Phys. **A623**, 471 (1997); Phys. Lett. **B438**, 9 (1998); Nucl. Phys. **A651**, 277 (1999) .
[54] J. E. Amaro, J. A. Caballero, T. W. Donnelly, A. M. Lallena, E. Moya de Guerra, and J. M. Udias, Nucl. Phys. **A602**, 263 (1996).
[55] P.-O. Löwdin, Phys. Rev. **97**, 1474 (1955).
[56] M. V. Stoitsov, A. N. Antonov, and S. S. Dimitrova, Phys. Rev. C **47**, R455 (1993); **48**, 74 (1993).
[57] J. E. Amaro, M. B. Barbaro, J. A. Caballero, T. W. Donnelly, and A. Molinari, Nucl. Phys. **A657**, 161 (1999).
[58] S. Galster *et al*., Nucl. Phys. **B32**, 221 (1971).
[59] R. M. Sealock *et al*., Phys. Rev. Lett. **62**, 1350 (1989).
[60] D. B. Day, J. S. McCarthy, Z. E. Meziani, R. Minehart, R. Sealock, S. T. Thornton, J. Jourdan, I. Sick, B. W. Filippone, R. D. McKeown, R. G. Milner, D. H. Potterveld, and Z. Szalata, Phys. Rev. C **48**, 1849 (1993).
[61] P. Barreau, M. Bernheim, J. Duclos, J. M. Finn, Z. Meziani, J. Morgenstern, J. Mougey, D. Royer, B. Saghai, D. Tarnowski, S. Turck-Chieze, M. Brussel, G. P. Capitani, E. De Sanctis, S. Frullani, F. Garibaldi, D. B. Isabelle, E. Jans, I. Sick, and P. D. Zimmerman, Nucl. Phys. **A402**, 515 (1983).
[62] R. R. Whitney, I. Sick, J. R. Ficenec, R. D. Kephart, and W. P. Trower, Phys. Rev. C **9**, 2230 (1974).
[63] J. S. O'Connell *et al*., Phys. Rev. C **35**, 1063 (1987).
[64] D. T. Baran *et al*., Phys. Rev. Lett. **61**, 400 (1988).
[65] G. Höhler *et al*., Nucl. Phys. **B114**, 505 (1976).